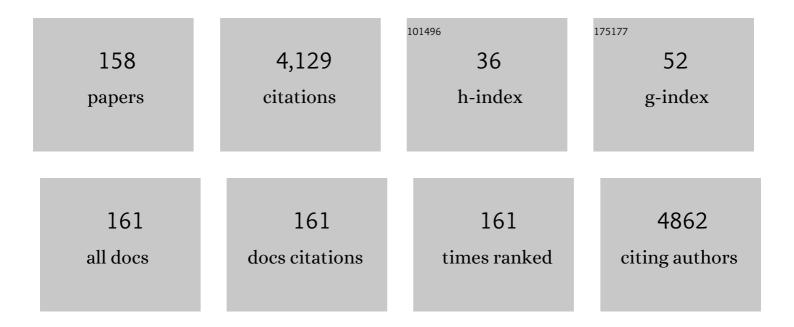
Mario Tyago Murakami

List of Publications by Year in descending order

Source: https://exaly.com/author-pdf/2588875/publications.pdf Version: 2024-02-01



#	Article	IF	CITATIONS
1	Enzymatic toxins from snake venom: structural characterization and mechanism of catalysis. FEBS Journal, 2011, 278, 4544-4576.	2.2	233
2	Recent advances in the understanding of brown spider venoms: From the biology of spiders to the molecular mechanisms of toxins. Toxicon, 2014, 83, 91-120.	0.8	116
3	Structural basis for glucose tolerance in GH1 β-glucosidases. Acta Crystallographica Section D: Biological Crystallography, 2014, 70, 1631-1639.	2.5	115
4	Inhibition of Myotoxic Activity of Bothrops asper Myotoxin II by the Anti-trypanosomal Drug Suramin. Journal of Molecular Biology, 2005, 350, 416-426.	2.0	106
5	Structural Basis for Metal Ion Coordination and the Catalytic Mechanism of Sphingomyelinases D. Journal of Biological Chemistry, 2005, 280, 13658-13664.	1.6	90
6	Batroxase, a new metalloproteinase from B. atrox snake venom with strong fibrinolytic activity. Toxicon, 2012, 60, 70-82.	0.8	85
7	Dissecting structure–function–stability relationships of a thermostable GH5-CBM3 cellulase from <i>Bacillus subtilis</i> 168. Biochemical Journal, 2012, 441, 95-104.	1.7	81
8	Plant Pathogenic Bacteria Utilize Biofilm Growth-associated Repressor (BigR), a Novel Winged-helix Redox Switch, to Control Hydrogen Sulfide Detoxification under Hypoxia. Journal of Biological Chemistry, 2011, 286, 26148-26157.	1.6	73
9	The Penicillium echinulatum Secretome on Sugar Cane Bagasse. PLoS ONE, 2012, 7, e50571.	1.1	70
10	Rational engineering of the Trichoderma reesei RUT-C30 strain into an industrially relevant platform for cellulase production. Biotechnology for Biofuels, 2020, 13, 93.	6.2	68
11	Structural insights into the catalytic mechanism of sphingomyelinases D and evolutionary relationship to glycerophosphodiester phosphodiesterases. Biochemical and Biophysical Research Communications, 2006, 342, 323-329.	1.0	63
12	Structure and Function of a Novel Cellulase 5 from Sugarcane Soil Metagenome. PLoS ONE, 2013, 8, e83635.	1.1	59
13	Interfacial surface charge and free accessibility to the PLA2-active site-like region are essential requirements for the activity of Lys49 PLA2 homologues. Toxicon, 2007, 49, 378-387.	0.8	58
14	Molecular Mechanisms Associated with Xylan Degradation by Xanthomonas Plant Pathogens. Journal of Biological Chemistry, 2014, 289, 32186-32200.	1.6	57
15	Oligomerization as a strategy for cold adaptation: Structure and dynamics of the GH1 β-glucosidase from Exiguobacterium antarcticum B7. Scientific Reports, 2016, 6, 23776.	1.6	57
16	Crystal structure of the platelet activator convulxin, a disulfide-linked α4β4 cyclic tetramer from the venom of Crotalus durissus terrificus. Biochemical and Biophysical Research Communications, 2003, 310, 478-482.	1.0	55
17	Biochemical and structural characterization of a β-1,3–1,4-glucanase from Bacillus subtilis 168. Process Biochemistry, 2011, 46, 1202-1206.	1.8	55
18	A novel cold-adapted and glucose-tolerant GH1 β-glucosidase from Exiguobacterium antarcticum B7. International Journal of Biological Macromolecules, 2016, 82, 375-380.	3.6	55

#	Article	IF	CITATIONS
19	Structural basis for branchingâ€enzyme activity of glycoside hydrolase family 57: Structure and stability studies of a novel branching enzyme from the hyperthermophilic archaeon <i>Thermococcus Kodakaraensis</i> KOD1. Proteins: Structure, Function and Bioinformatics, 2011, 79, 547-557.	1.5	54
20	Engineering Bifunctional Laccase-Xylanase Chimeras for Improved Catalytic Performance. Journal of Biological Chemistry, 2011, 286, 43026-43038.	1.6	52
21	Structure of a novel class II phospholipase D: Catalytic cleft is modified by a disulphide bridge. Biochemical and Biophysical Research Communications, 2011, 409, 622-627.	1.0	49
22	Correlation of temperature induced conformation change with optimum catalytic activity in the recombinant G/11 xylanase A fromBacillus subtilisstrain 168 (1A1). FEBS Letters, 2005, 579, 6505-6510.	1.3	46
23	Isolation, characterization and biological activity of acidic phospholipase A2 isoforms from Bothrops jararacussu snake venom. Biochimie, 2003, 85, 983-991.	1.3	45
24	Functional characterization and oligomerization of a recombinant xyloglucan-specific endo-β-1,4-glucanase (GH12) from Aspergillus niveus. Biochimica Et Biophysica Acta - Proteins and Proteomics, 2012, 1824, 461-467.	1.1	45
25	Crystal structure and biochemical characterization of the recombinant ThBgl, a GH1 β-glucosidase overexpressed in Trichoderma harzianum under biomass degradation conditions. Biotechnology for Biofuels, 2016, 9, 71.	6.2	45
26	Thrombomodulin-independent Activation of Protein C and Specificity of Hemostatically Active Snake Venom Serine Proteinases. Journal of Biological Chemistry, 2005, 280, 39309-39315.	1.6	43
27	Mode of operation and low-resolution structure of a multi-domain and hyperthermophilic endo-β-1,3-glucanase from Thermotoga petrophila. Biochemical and Biophysical Research Communications, 2011, 406, 590-594.	1.0	43
28	How pH Modulates the Dimer-Decamer Interconversion of 2-Cys Peroxiredoxins from the Prx1 Subfamily. Journal of Biological Chemistry, 2015, 290, 8582-8590.	1.6	43
29	Crystal structure of mature 2S albumin from Moringa oleifera seeds. Biochemical and Biophysical Research Communications, 2015, 468, 365-371.	1.0	43
30	Molecular insights into substrate specificity and thermal stability of a bacterial GH5-CBM27 endo-1,4-β-d-mannanase. Journal of Structural Biology, 2012, 177, 469-476.	1.3	42
31	Effects of the linker region on the structure and function of modular GH5 cellulases. Scientific Reports, 2016, 6, 28504.	1.6	40
32	The repeat domain of the type III effector protein PthA shows a TPRâ€like structure and undergoes conformational changes upon DNA interaction. Proteins: Structure, Function and Bioinformatics, 2010, 78, 3386-3395.	1.5	39
33	A structure based model for liposome disruption and the role of catalytic activity in myotoxic phospholipase A2s. Toxicon, 2003, 42, 903-913.	0.8	38
34	SMase II, a new sphingomyelinase D from Loxosceles laeta venom gland: Molecular cloning, expression, function and structural analysis. Toxicon, 2009, 53, 743-753.	0.8	38
35	Molecular characterization of an acidic phospholipase A2 from Bothrops pirajai snake venom: synthetic C-terminal peptide identifies its antiplatelet region. Archives of Toxicology, 2011, 85, 1219-1233.	1.9	38
36	Structural studies of BmooMPα-I, a non-hemorrhagic metalloproteinase from Bothrops moojeni venom. Toxicon, 2010, 55, 361-368.	0.8	37

#	Article	IF	CITATIONS
37	Structure of the polypeptide crotamine from the Brazilian rattlesnake <i>Crotalus durissus terrificus</i> . Acta Crystallographica Section D: Biological Crystallography, 2013, 69, 1958-1964.	2.5	37
38	Purification, characterization and crystallization of Jararacussin-I, a fibrinogen-clotting enzyme isolated from the venom of Bothrops jararacussu. Toxicon, 2002, 40, 1307-1312.	0.8	36
39	Intermolecular Interactions and Characterization of the Novel Factor Xa Exosite Involved in Macromolecular Recognition and Inhibition: Crystal Structure of Human Gla-domainless Factor Xa Complexed with the Anticoagulant Protein NAPc2 from the Hematophagous Nematode Ancylostoma caninum, Journal of Molecular Biology, 2007, 366, 602-610.	2.0	36
40	Thermal-induced conformational changes in the product release area drive the enzymatic activity of xylanases 10B: Crystal structure, conformational stability and functional characterization of the xylanase 10B from Thermotoga petrophila RKU-1. Biochemical and Biophysical Research Communications, 2010, 403, 214-219.	1.0	36
41	Molecular adaptability of nucleoside diphosphate kinase b from trypanosomatid parasites: stability, oligomerization and structural determinants of nucleotide binding. Molecular BioSystems, 2011, 7, 2189.	2.9	36
42	An engineered GH1 β-glucosidase displays enhanced glucose tolerance and increased sugar release from lignocellulosic materials. Scientific Reports, 2019, 9, 4903.	1.6	36
43	Gene cloning, expression and biochemical characterization of a glucose- and xylose-stimulated β-glucosidase from Humicola insolens RP86. Journal of Molecular Catalysis B: Enzymatic, 2014, 106, 1-10.	1.8	33
44	The molecular motor Myosin Va interacts with the cilia-centrosomal protein RPGRIP1L. Scientific Reports, 2017, 7, 43692.	1.6	33
45	Assembling a xylanase–lichenase chimera through all-atom molecular dynamics simulations. Biochimica Et Biophysica Acta - Proteins and Proteomics, 2013, 1834, 1492-1500.	1.1	32
46	Cloning, heterologous expression and biochemical characterization of a non-specific endoglucanase family 12 from Aspergillus terreus NIH2624. Biochimica Et Biophysica Acta - Proteins and Proteomics, 2017, 1865, 395-403.	1.1	32
47	An actinobacteria lytic polysaccharide monooxygenase acts on both cellulose and xylan to boost biomass saccharification. Biotechnology for Biofuels, 2019, 12, 117.	6.2	31
48	Crystal structure of an acidic platelet aggregation inhibitor and hypotensive phospholipase A2 in the monomeric and dimeric states: insights into its oligomeric state. Biochemical and Biophysical Research Communications, 2004, 323, 24-31.	1.0	30
49	Structural Insights into Functional Overlapping and Differentiation among Myosin V Motors. Journal of Biological Chemistry, 2013, 288, 34131-34145.	1.6	29
50	Development of a chimeric hemicellulase to enhance the xylose production and thermotolerance. Enzyme and Microbial Technology, 2015, 69, 31-37.	1.6	29
51	Active site mapping of Loxosceles phospholipases D: Biochemical and biological features. Biochimica Et Biophysica Acta - Molecular and Cell Biology of Lipids, 2016, 1861, 970-979.	1.2	29
52	The mechanism by which a distinguishing arabinofuranosidase can cope with internal di-substitutions in arabinoxylans. Biotechnology for Biofuels, 2018, 11, 223.	6.2	29
53	Development and Biotechnological Application of a Novel Endoxylanase Family GH10 Identified from Sugarcane Soil Metagenome. PLoS ONE, 2013, 8, e70014.	1.1	28
54	The structure of a native <scp>l</scp> -amino acid oxidase, the major component of the Vipera ammodytes ammodytes venomic, reveals dynamic active site and quaternary structure stabilization by divalent ions. Molecular BioSystems, 2011, 7, 379-384.	2.9	27

#	Article	IF	CITATIONS
55	Effects of High Pressure Homogenization on the Activity, Stability, Kinetics and Three-Dimensional Conformation of a Glucose Oxidase Produced by Aspergillus niger. PLoS ONE, 2014, 9, e103410.	1.1	27
56	Two distinct catalytic pathways for GH43 xylanolytic enzymes unveiled by X-ray and QM/MM simulations. Nature Communications, 2021, 12, 367.	5.8	27
57	A Redox 2-Cys Mechanism Regulates the Catalytic Activity of Divergent Cyclophilins Â. Plant Physiology, 2013, 162, 1311-1323.	2.3	26
58	Xylan-specific carbohydrate-binding module belonging to family 6 enhances the catalytic performance of a GH11 endo-xylanase. New Biotechnology, 2016, 33, 467-472.	2.4	26
59	Xyloglucan processing machinery in Xanthomonas pathogens and its role in the transcriptional activation of virulence factors. Nature Communications, 2021, 12, 4049.	5.8	26
60	Gut microbiome of the largest living rodent harbors unprecedented enzymatic systems to degrade plant polysaccharides. Nature Communications, 2022, 13, 629.	5.8	26
61	Active and Exo-site Inhibition of Human Factor Xa: Structure of des-Gla Factor Xa Inhibited by NAP5, a Potent Nematode Anticoagulant Protein from Ancylostoma caninum. Journal of Molecular Biology, 2007, 371, 774-786.	2.0	25
62	The accessory domain changes the accessibility and molecular topography of the catalytic interface in monomeric GH39 β-xylosidases. Acta Crystallographica Section D: Biological Crystallography, 2012, 68, 1339-1345.	2.5	25
63	Structural insights into selectivity and cofactor binding in snake venom l-amino acid oxidases. Biochemical and Biophysical Research Communications, 2012, 421, 124-128.	1.0	25
64	In Vitro, In Vivo and In Silico Analysis of the Anticancer and Estrogen-like Activity of Guava Leaf Extracts. Current Medicinal Chemistry, 2014, 21, 2322-2330.	1.2	25
65	Enhanced xyloglucan-specific endo-β-1,4-glucanase efficiency in an engineered CBM44-XegA chimera. Applied Microbiology and Biotechnology, 2015, 99, 5095-5107.	1.7	25
66	Kinase Inhibitor Profile for Human Nek1, Nek6, and Nek7 and Analysis of the Structural Basis for Inhibitor Specificity. Molecules, 2015, 20, 1176-1191.	1.7	24
67	Structure and function of a novel GH8 endoglucanase from the bacterial cellulose synthase complex of Raoultella ornithinolytica. PLoS ONE, 2017, 12, e0176550.	1.1	24
68	Substrate cleavage pattern, biophysical characterization and low-resolution structure of a novel hyperthermostable arabinanase from Thermotoga petrophila. Biochemical and Biophysical Research Communications, 2010, 399, 505-511.	1.0	23
69	Structural Basis for Xyloglucan Specificity and α- <scp>d</scp> -Xyl <i>p</i> (1 →) Tj ETQq1 1 0.784314 rgBT /Ov 1930-1942.	verlock 10 1.2	Tf 50 187 Td 23
70	Insights into metal ion binding inÂphospholipases A2: ultra high-resolution crystal structures ofÂanÂacidic phospholipase A2 inÂtheÂCa2+ free andÂbound states. Biochimie, 2006, 88, 543-549.	1.3	22
71	Structure of a novel thermostable GH51 α‣â€arabinofuranosidase from <i>Thermotoga petrophila</i> RKUâ€1. Protein Science, 2011, 20, 1632-1637.	3.1	22
72	Two structurally discrete GH7-cellobiohydrolases compete for the same cellulosic substrate fiber. Biotechnology for Biofuels, 2012, 5, 21.	6.2	22

#	Article	IF	CITATIONS
73	Crystal structure of β1→6â€galactosidase from <i>Bifidobacterium bifidum</i> S17: trimeric architecture, molecular determinants of the enzymatic activity and its inhibition by αâ€galactose. FEBS Journal, 2016, 283, 4097-4112.	2.2	22
74	Crystal Structure and Regulation of the Citrus Pol III Repressor MAF1 by Auxin and Phosphorylation. Structure, 2017, 25, 1360-1370.e4.	1.6	22
75	Functional characterization and comparative analysis of two heterologous endoglucanases from diverging subfamilies of glycosyl hydrolase family 45. Enzyme and Microbial Technology, 2019, 120, 23-35.	1.6	22
76	Functional and structural analysis of two fibrinogen-activating enzymes isolated from the venoms of <italic>Crotalus durissus terrificus</italic> and <italic>Crotalus durissus collilineatus</italic> . Acta Biochimica Et Biophysica Sinica, 2009, 41, 21-29.	0.9	21
77	Molecular cloning and biochemical characterization of a myotoxin inhibitor from Bothrops alternatus snake plasma. Biochimie, 2011, 93, 583-592.	1.3	21
78	Mechanistic Strategies for Catalysis Adopted by Evolutionary Distinct Family 43 Arabinanases. Journal of Biological Chemistry, 2014, 289, 7362-7373.	1.6	21
79	Kinetic and mechanistic characterization of the Sphingomyelinases D from Loxosceles intermedia spider venom. Toxicon, 2006, 47, 380-386.	0.8	19
80	Functional and biophysical characterization of a hyperthermostable GH51 α-l-arabinofuranosidase from Thermotoga petrophila. Biotechnology Letters, 2011, 33, 131-137.	1.1	19
81	Crystal structure of Jararacussinâ€l. The highly negatively charged catalytic interface contributes to macromolecular selectivity in snake venom thrombinâ€like enzymes. Protein Science, 2013, 22, 128-132.	3.1	19
82	Structural insights into β-1,3-glucan cleavage by a glycoside hydrolase family. Nature Chemical Biology, 2020, 16, 920-929.	3.9	19
83	Structural studies of the Trypanosoma cruzi Old Yellow Enzyme: Insights into enzyme dynamics and specificity. Biophysical Chemistry, 2013, 184, 44-53.	1.5	18
84	Effect of dynamic high pressure on functional and structural properties of bovine serum albumin. Food Research International, 2017, 99, 748-754.	2.9	18
85	N-glycan Utilization by Bifidobacterium Gut Symbionts Involves a Specialist β-Mannosidase. Journal of Molecular Biology, 2019, 431, 732-747.	2.0	18
86	Reduction of sulfenic acids by ascorbate in proteins, connecting thiol-dependent to alternative redox pathways. Free Radical Biology and Medicine, 2020, 156, 207-216.	1.3	18
87	Crystallographic portrayal of different conformational states of a Lys49 phospholipase A2 homologue: Insights into structural determinants for myotoxicity and dimeric configuration. International Journal of Biological Macromolecules, 2012, 51, 209-214.	3.6	17
88	P-I class metalloproteinase from Bothrops moojeni venom is a post-proline cleaving peptidase with kininogenase activity: Insights into substrate selectivity and kinetic behavior. Biochimica Et Biophysica Acta - Proteins and Proteomics, 2014, 1844, 545-552.	1.1	17
89	Crystal structure of a novel myotoxic Arg49 phospholipase A2 homolog (zhaoermiatoxin) from Zhaoermia mangshanensis snake venom: Insights into Arg49 coordination and the role of Lys122 in the polarization of the C-terminus. Toxicon, 2008, 51, 723-735.	0.8	16
90	Adaptive evolution in the toxicity of a spider's venom enzymes. BMC Evolutionary Biology, 2015, 15, 290.	3.2	16

#	Article	IF	CITATIONS
91	Structural basis of exo-β-mannanase activity in the GH2 family. Journal of Biological Chemistry, 2018, 293, 13636-13649.	1.6	16
92	Targeting <i>Loxosceles</i> spider Sphingomyelinase D with small-molecule inhibitors as a potential therapeutic approach for loxoscelism. Journal of Enzyme Inhibition and Medicinal Chemistry, 2019, 34, 310-321.	2.5	16
93	Structural Insights into Substrate Binding of Brown Spider Venom Class II Phospholipases D. Current Protein and Peptide Science, 2015, 16, 768-774.	0.7	16
94	Structureâ€guided design combined with evolutionary diversity led to the discovery of the xyloseâ€releasing exoâ€xylanase activity in the glycoside hydrolase family 43. Biotechnology and Bioengineering, 2019, 116, 734-744.	1.7	15
95	Purification, Biochemical and Functional Characterization of Miliin, a New Thiol-Dependent Serine Protease Isolated from the Latex of Euphorbia milii. Protein and Peptide Letters, 2008, 15, 724-730.	0.4	14
96	How high pressure pre-treatments affect the function and structure of hen egg-white lysozyme. Innovative Food Science and Emerging Technologies, 2018, 47, 195-203.	2.7	14
97	Biochemical and Structural Investigations of Bothropstoxin-II, a Myotoxic Asp49 Phospholipase A2 from Bothrops jararacussu Venom. Protein and Peptide Letters, 2008, 15, 1002-1008.	0.4	13
98	Crystallization and preliminary X-ray diffraction analysis of a class II phospholipase D from <i>Loxosceles intermedia</i> venom. Acta Crystallographica Section F: Structural Biology Communications, 2011, 67, 234-236.	0.7	13
99	Expression, purification and spectroscopic analysis of an HdrC: An iron–sulfur cluster-containing protein from Acidithiobacillus ferrooxidans. Process Biochemistry, 2011, 46, 1335-1341.	1.8	13
100	Crystal structure of Staphylococcus aureus exfoliative toxin D-like protein: Structural basis for the high specificity of exfoliative toxins. Biochemical and Biophysical Research Communications, 2015, 467, 171-177.	1.0	13
101	A Novel Fungal Lipase With Methanol Tolerance and Preference for Macaw Palm Oil. Frontiers in Bioengineering and Biotechnology, 2020, 8, 304.	2.0	13
102	Characterization of a Hexameric Exo-Acting GH51 $\hat{1}\pm$ -l-Arabinofuranosidase from the Mesophilic Bacillus subtilis. Molecular Biotechnology, 2013, 55, 260-267.	1.3	12
103	Correlation between catalysis and tertiary structure arrangement in an archaeal halophilic subtilase. Biochimie, 2012, 94, 798-805.	1.3	11
104	A novel β-glucosidase isolated from the microbial metagenome of Lake Poraquê (Amazon, Brazil). Biochimica Et Biophysica Acta - Proteins and Proteomics, 2018, 1866, 569-579.	1.1	11
105	Luciferase isozymes from the Brazilian Aspisoma lineatum (Lampyridae) firefly: origin of efficient pH-sensitive lantern luciferases from fat body pH-insensitive ancestors. Photochemical and Photobiological Sciences, 2020, 19, 1750-1764.	1.6	11
106	Exploring the Molecular Basis for Substrate Affinity and Structural Stability in Bacterial GH39 β-Xylosidases. Frontiers in Bioengineering and Biotechnology, 2020, 8, 419.	2.0	11
107	Structure of myotoxin II, a catalytically inactive Lys49 phospholipase A2homologue fromAtropoides nummifervenom. Acta Crystallographica Section F: Structural Biology Communications, 2006, 62, 423-426.	0.7	10
108	Expression, purification, crystallization and preliminary crystallographic analysis of an endo-1,5-α- <scp>L</scp> -arabinanase from hyperthermophilic <i>Thermotoga petrophila</i> . Acta Crystallographica Section F: Structural Biology Communications, 2009, 65, 902-905.	0.7	10

#	Article	IF	CITATIONS
109	Insights into Phosphate Cooperativity and Influence of Substrate Modifications on Binding and Catalysis of Hexameric Purine Nucleoside Phosphorylases. PLoS ONE, 2012, 7, e44282.	1.1	10
110	Pyrrole-indolinone SU11652 targets the nucleoside diphosphate kinase from Leishmania parasites. Biochemical and Biophysical Research Communications, 2017, 488, 461-465.	1.0	10
111	Calcium and magnesium ions modulate the oligomeric state and function of mitochondrial 2-Cys peroxiredoxins in Leishmania parasites. Journal of Biological Chemistry, 2017, 292, 7023-7039.	1.6	10
112	Crystallization and preliminary X-ray crystallographic analysis of the heterodimeric crotoxin complex and the isolated subunits crotapotin and phospholipase A2. Acta Crystallographica Section F: Structural Biology Communications, 2007, 63, 287-290.	0.7	9
113	Spatially remote motifs cooperatively affect substrate preference of a ruminal GH26-type endo-β-1,4-mannanase. Journal of Biological Chemistry, 2020, 295, 5012-5021.	1.6	9
114	Identification of a cold-adapted and metal-stimulated β-1,4-glucanase with potential use in the extraction of bioactive compounds from plants. International Journal of Biological Macromolecules, 2021, 166, 190-199.	3.6	9
115	Cloning, expression, purification, crystallization and preliminary X-ray diffraction studies of the catalytic domain of a hyperthermostable endo-1,4-l²- <scp>D</scp> -mannanase from <i>Thermotoga petrophila</i> RKU-1. Acta Crystallographica Section F: Structural Biology Communications, 2010, 66, 1078-1081.	0.7	8
116	The small heat shock proteins from Acidithiobacillus ferrooxidans: gene expression, phylogenetic analysis, and structural modeling. BMC Microbiology, 2011, 11, 259.	1.3	8
117	Crystallization and preliminary X-ray diffraction analysis of anL-amino-acid oxidase fromBothrops jararacussuvenom. Acta Crystallographica Section F: Structural Biology Communications, 2012, 68, 211-213.	0.7	8
118	Crystallization and preliminary X-ray diffraction studies of an <scp>L</scp> -amino-acid oxidase from <i>Lachesis muta</i> venom. Acta Crystallographica Section F, Structural Biology Communications, 2014, 70, 1556-1559.	0.4	8
119	Crystallization and preliminary X-ray diffraction analysis of a novel sphingomyelinase D fromLoxosceles gauchovenom. Acta Crystallographica Section F, Structural Biology Communications, 2014, 70, 1418-1420.	0.4	8
120	Adenosine Kinase couples sensing of cellular potassium depletion to purine metabolism. Scientific Reports, 2018, 8, 11988.	1.6	8
121	Crystal Structure of Bucain, a Three-Fingered Toxin from the Venom of the Malayan Krait (Bungarus) Tj ETQq1 1	0.784314 0.4	rgBT /Overloo
122	The Water Effect on the Kinetics of the Bovine Liver Catalase. Protein and Peptide Letters, 2011, 18, 879-885.	0.4	7
123	Crystal structure and biophysical characterization of the nucleoside diphosphate kinase from Leishmania braziliensis. BMC Structural Biology, 2015, 15, 2.	2.3	7
124	New contributions for industrial n-butanol fermentation: An optimized Clostridium strain and the use of xylooligosaccharides as a fermentation additive. Biomass and Bioenergy, 2018, 119, 304-313.	2.9	7
125	Unveiling the interaction between the molecular motor Myosin Vc and the small GTPase Rab3A. Journal of Proteomics, 2020, 212, 103549.	1.2	7
126	Voices of chemical biology. Nature Chemical Biology, 2021, 17, 1-4.	3.9	7

#	Article	IF	CITATIONS
127	Crystallization and preliminary X-ray diffraction analysis of suramin, a highly charged polysulfonated napthylurea, complexed with a myotoxic PLA2 from Bothrops asper venom. Biochimica Et Biophysica Acta - Proteins and Proteomics, 2004, 1703, 83-85.	1.1	6
128	Purification, crystallization and preliminary X-ray diffraction analysis of a class P-III metalloproteinase (BmMP-III) from the venom of <i>Bothrops moojeni</i> . Acta Crystallographica Section F: Structural Biology Communications, 2012, 68, 1222-1225.	0.7	6
129	The role of the C-terminus and Kpn loop in the quaternary structure stability of nucleoside diphosphate kinase from Leishmania parasites. Journal of Structural Biology, 2015, 192, 336-341.	1.3	6
130	A comparative structural analysis reveals distinctive features of co-factor binding and substrate specificity in plant aldo-keto reductases. Biochemical and Biophysical Research Communications, 2016, 474, 696-701.	1.0	6
131	Bacterial and Arachnid Sphingomyelinases D: Comparison of Biophysical and Pathological Activities. Journal of Cellular Biochemistry, 2017, 118, 2053-2063.	1.2	6
132	Crystal structure of a novel xylose isomerase from Streptomyces sp. F-1 revealed the presence of unique features that differ from conventional classes. Biochimica Et Biophysica Acta - General Subjects, 2020, 1864, 129549.	1.1	6
133	Crystallization and preliminary crystallographic analysis of SMase I, a sphingomyelinase fromLoxosceles laetaspider venom. Acta Crystallographica Section D: Biological Crystallography, 2004, 60, 1112-1114.	2.5	5
134	Crystallization and high-resolution X-ray diffraction data collection of an Asp49 PLA2 from Bothrops jararacussu venom both in the presence and absence of Ca2+ ions. Biochimica Et Biophysica Acta - Proteins and Proteomics, 2004, 1703, 79-81.	1.1	5
135	Cloning, expression, purification, crystallization and preliminary X-ray diffraction analysis of the mitochondrial tryparedoxin peroxidase from <i>Leishmania braziliensis</i> . Acta Crystallographica Section F: Structural Biology Communications, 2013, 69, 408-411.	0.7	5
136	Structure and Mechanism of Dimer–Monomer Transition of a Plant Poly(A)-Binding Protein upon RNA Interaction: Insights into Its Poly(A) Tail Assembly. Journal of Molecular Biology, 2015, 427, 2491-2506.	2.0	5
137	A rationally identified marine GH1 βâ€glucosidase has distinguishing functional features for simultaneous saccharification and fermentation. Biofuels, Bioproducts and Biorefining, 2020, 14, 1163-1179.	1.9	5
138	Crystallization and preliminary X-ray crystallographic studies of the mesophilic xylanase A fromBacillus subtilis1A1. Acta Crystallographica Section F: Structural Biology Communications, 2005, 61, 219-220.	0.7	4
139	Biophysical and Structural Characterization of the Recombinant Human elF3L. Protein and Peptide Letters, 2013, 21, 56-62.	0.4	4
140	The dark and bright sides of an enzyme: a three dimensional structure of the N-terminal domain of Zophobas morio luciferase-like enzyme, inferences on the biological function and origin of oxygenase/luciferase activity. Photochemical and Photobiological Sciences, 2016, 15, 654-665.	1.6	4
141	Tyrosine binding and promiscuity in the arginine repressor from the pathogenic bacterium Corynebacterium pseudotuberculosis. Biochemical and Biophysical Research Communications, 2016, 475, 350-355.	1.0	4
142	Substrate and Product-Assisted Catalysis: Molecular Aspects behind Structural Switches along Organic Hydroperoxide Resistance Protein Catalytic Cycle. ACS Catalysis, 2020, 10, 6587-6602.	5.5	4
143	Production, purification, crystallization and preliminary X-ray diffraction studies of the nucleoside diphosphate kinase b fromLeishmania major. Acta Crystallographica Section F: Structural Biology Communications, 2009, 65, 1116-1119.	0.7	3
144	Molecular cloning, overexpression, purification, crystallization and preliminary X-ray diffraction analysis of a purine nucleoside phosphorylase fromBacillus subtilisstrain 168. Acta Crystallographica Section F: Structural Biology Communications, 2011, 67, 618-622.	0.7	3

#	Article	IF	CITATIONS
145	Myosin Va interacts with the exosomal protein spermine synthase. Bioscience Reports, 2019, 39, .	1.1	3
146	Cloning of a Novel Feruloyl Esterase from Rumen Microbial Metagenome for Substantial Yield of Mono- and Diferulic Acids from Natural Substrates. Protein and Peptide Letters, 2015, 22, 681-688.	0.4	3
147	Initial structural analysis of an α4β4C-type lectin from the venom ofCrotalus durissus terrificus. Acta Crystallographica Section D: Biological Crystallography, 2003, 59, 1813-1815.	2.5	2
148	Crystallization and preliminary X-ray crystallographic studies of Protac®, a commercial protein C activator isolated from Agkistrodon contortrix contortrix venom. Biochimica Et Biophysica Acta - Proteins and Proteomics, 2005, 1752, 202-204.	1.1	2
149	Crystallization and preliminary X-ray diffraction analysis of a novel Arg49 phospholipase A2homologue fromZhaoermia mangshanensisvenom. Acta Crystallographica Section F: Structural Biology Communications, 2007, 63, 605-607.	0.7	2
150	Biophysical Characterization of Alanine Aminotransferase from Trypanosoma cruzi. Protein and Peptide Letters, 2016, 23, 1118-1122.	0.4	2
151	Analysis of peptidase activities of a cathepsin B-like (TcoCBc1) from Trypanosoma congolense. Biochimica Et Biophysica Acta - Proteins and Proteomics, 2014, 1844, 1260-1267.	1.1	1
152	Molecular cloning, overexpression, purification and crystallographic analysis of a GH43 β-xylosidase from <i>Bacillus licheniformis</i> . Acta Crystallographica Section F, Structural Biology Communications, 2015, 71, 962-965.	0.4	1
153	In-solution behavior and protective potential of asparagine synthetase A from Trypanosoma cruzi. Molecular and Biochemical Parasitology, 2019, 230, 1-7.	0.5	1
154	Influence of the C-terminal domain on the bioluminescence activity and color determination in green and red emitting beetle luciferases and luciferase-like enzyme. Photochemical and Photobiological Sciences, 2021, 20, 113-122.	1.6	1
155	Crystallization and preliminary X-ray diffraction analysis of a new xyloglucanase fromXanthomonas campestrispv.campestris. Acta Crystallographica Section F: Structural Biology Communications, 2013, 69, 676-678.	0.7	Ο
156	Protein C Activators from Snake Venom. , 2013, , 3045-3048.		0
157	A single P115Q mutation modulates specificity in the Corynebacterium pseudotuberculosis arginine repressor. Biochimica Et Biophysica Acta - General Subjects, 2020, 1864, 129597.	1.1	0
158	Structure of the class XI myosin globular tail reveals evolutionary hallmarks for cargo recognition in plants. Acta Crystallographica Section D: Structural Biology, 2021, 77, 522-533.	1.1	0